Journal of Nuclear Materials 494 (2017) 87–94

Contents lists available at ScienceDirect

Journal of Nuclear Materials

journal homepage: www.elsevier.com/locate/jnucmat

Modelling the radiolytic corrosion of α-doped UO_2 and spent nuclear fuel

Nazhen Liu [a], Zack Qin [a], James J. Noël [a, b, *], David W. Shoesmith [a, b, **]

[a] Department of Chemistry, The University of Western Ontario, London, Ontario, N6A 5B7, Canada
[b] Surface Science Western, The University of Western Ontario, London, Ontario, N6G 0J3, Canada

HIGHLIGHTS

- A model is adapted to simulate the corrosion rates measured on α-doped UO_2.
- Simulated corrosion rates are in good agreement with the published rates.
- The corrosion rate is determined by the radiolytic production rate of H_2O_2.
- The accumulation of O_2 leads to an increase in corrosion rate in a closed system.
- The corrosion rate decreases to a negligible level by including H_2 effect.

ARTICLE INFO

Article history:
Received 7 March 2017
Received in revised form
26 May 2017
Accepted 6 July 2017
Available online 8 July 2017

Keywords:
α-Doped UO_2
Spent nuclear fuel
Waste disposal
Modelling

ABSTRACT

A model previously developed to predict the corrosion rate of spent fuel (UO_2) inside a failed waste container has been adapted to simulate the rates measured on a wide range of α-doped UO_2 and spent fuel specimens. This simulation confirms the validity of the model and demonstrates that the steady-state corrosion rate is controlled by the radiolytic production of H_2O_2 (which has been shown to be the primary oxidant driving fuel corrosion), irrespective of the reactivity of the UO_2 matrix. The model was then used to determine the consequences of corrosion inside a failed container resealed by steel corrosion products. The possible accumulation of O_2, produced by H_2O_2 decomposition, was found to accelerate the corrosion rate in a closed system. However, the simultaneous accumulation of radiolytic H_2, which is activated as a reductant on the noble metal (ε) particles in the spent fuel, rapidly overcame this acceleration leading to the eventual suppression of the corrosion rate to insignificant values. Calculations also showed that, while the radiation dose rate, the H_2O_2 decomposition ratio, and the surface coverage of ε particles all influenced the short term corrosion rate, the influence of the radiolytically produced H_2 was the overwhelming influence in reducing the rate to negligible level (i.e., $<10^{-20}$ mol m^{-2} s^{-1}).

1. Introduction

If nuclear energy is to play an important role in alleviating the risk of global climate change, it must be demonstrated that the high level waste can be safely disposed of. The approved approach for the long-term management of used nuclear fuel in Canada is disposal in a deep geologic repository (DGR) [1,2]. As accepted internationally, the repository concept is based on multiple barriers including the fuel bundles, durable metal containers, a clay buffer and seals around the container, and a deep geologic formation [3]. A key barrier is the corrosion-resistant container which is expected to isolate the used fuel for a very long time [4,5]. However, it is judicious to examine the consequences of container failure and the exposure of used fuel bundles to groundwater. In the anoxic conditions anticipated in a DGR, H_2O radiolysis resulting from the radiation fields associated with the used fuel within a failed container will be the only source of oxidants. The radiolysis product, H_2O_2, has been shown to be the primary oxidant driving fuel corrosion [6,7]. Oxidation of fuel (U^{IV}) will produce the oxidized form (U^{VI})

* Corresponding author. Department of Chemistry, The University of Western Ontario, London, Ontario, N6A 5B7, Canada.
** Corresponding author. Department of Chemistry, The University of Western Ontario, London, Ontario, N6A 5B7, Canada.
E-mail addresses: jjnoel@uwo.ca (J.J. Noël), dwshoesm@uwo.ca (D.W. Shoesmith).

http://dx.doi.org/10.1016/j.jnucmat.2017.07.011
0022-3115/

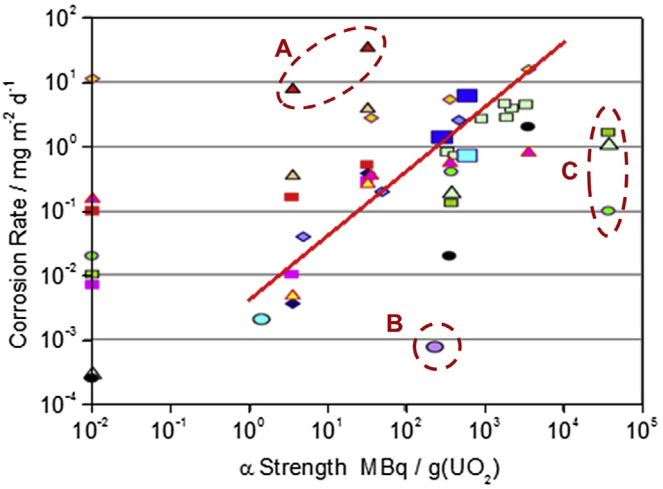

Fig. 1. Corrosion rates of α-doped UO_2, non-doped UO_2 (0.01 MBq g^{-1} (UO_2)), SIMFUEL and some spent fuels (from Ref. [17], with permission). The red line indicates a linear least squares fit to the data from Ref. [18] without including values marked A, B and C, which are discussed in the text. (For interpretation of the references to colour in this figure legend, the reader is referred to the web version of this article.)

with a considerably higher solubility, leading to the release of radionuclides [8].

Since α-radiolysis of H_2O is the dominant source of oxidants for spent fuel oxidation/dissolution (corrosion) inside a failed waste nuclear container, the influence of the α-dose rate on the corrosion of UO_2 materials has been extensively studied [9–16]. The corrosion rates as a function of α-dose from a range of studies have been discussed in detail and summarized [17]. These measurements were conducted on a number of specimens including ^{233}U-doped UO_2, ^{238}Pu-doped UO_2, ^{225}Ac-doped UO_2, UO_2 fuel pellets, SIMFUEL and spent fuels. Fig. 1 shows that, while significant variability exists, a clear trend of increasing corrosion rate with increasing alpha source strength was established. It was suggested that for alpha source strengths below ~1 MBq g^{-1} (UO_2), the influence of α-radiolysis became insignificant, the fuel dissolution rate becoming chemically controlled with U released in the unoxidized U^{IV} state.

Within this compilation, three sets of data, marked A, B and C, cannot be considered to fit the linear relationship. For A, corrosion rates were calculated based on electrochemical impedance spectroscopy measurements which required the compensation of the resistance in low conductivity materials. This led to large errors and an overestimation of the rates. The value labelled B was measured in a clay environment known to contain reducing species leading to the unexpectedly low values. The values labelled C were measured on ^{238}Pu-doped specimens, and it has been suggested, but not proven, that the low rates indicate a stabilizing influence of Pu on the UO_2 matrix. The line in Fig. 1 shows a fit to the data (excluding the data marked A, B and C) used by the Nuclear Waste Management Organization (Toronto, Canada) in repository performance assessment calculations [18] yielding the relationship,

$$\text{Corrosion Rate (mg (UO}_2\text{) m}^{-2}\text{ d}^{-1}\text{)} = 4.35 \times 10^{-3} \times \text{Activity (MBq g}^{-1}\text{ (UO}_2\text{))}$$

The errors associated with the use of this fit have been discussed elsewhere [18].

In this study, an attempt is made to use these data to validate the model we have developed for fuel corrosion inside a failed waste container [19–22]. The model is then used to evaluate a number of scenarios which could occur within a failed container. Of particular interest is the influence of O_2, which can be produced by both decomposition of H_2O_2 and water radiolysis. In many of the experiments performed to produce the rates plotted in Fig. 1, the system was open and/or the solution purged with inert gas, making it possible that O_2 formed within the experiment could have influenced the corrosion rate measured. Although inadvertently achieved, this could have simulated the conditions achievable within a failed container possibly resealed by the accumulation of container corrosion products. The consequences of such a scenario are also addressed in this study.

2. Description of models

2.1. Conversion of α-source strength to α-dose rate

In Fig. 1 the corrosion rates are plotted as a function of alpha-source strength. The specific alpha-source strength is converted to the alpha-dose rate to the water layer adjacent to the UO_2 surface, which is used in the model to calculate the rate of production of radiolytic species. The rate of radiolytic production for species i can be calculated according to equation (1),

$$R_i\left(\text{mol m}^{-3}\text{ s}^{-1}\right) = D_R \times g_i \times \rho_{H_2O} \quad (1)$$

where D_R is the dose rate representing the rate of energy deposition per unit of mass, g_i is the g-value of species i (the number of moles formed per joule of radiation energy absorbed), and ρ_{H_2O} is the density of water.

For α-radiation, the dose rate near the solid surface and the energy fraction transferred into the solution can be approximately estimated from geometric considerations. Since the transfer range of α-emissions in UO_2 is ~14 μm, only a fraction of the α-particles within this range can reach the adjacent liquid to form radiolytic products [17]. For a 1 MBq g^{-1} (UO_2) doped UO_2, the energy deposited in the UO_2 layer with a thickness of 14 μm is 1.425×10^{-8} J cm^{-2} s^{-1}, according to equation (2),

$$\text{Total Energy Deposition in a 14 μm UO}_2\text{ layer}\left(\text{corresponding to }\frac{1\text{MBq}}{\text{g (UO}_2\text{)}}\right) = \text{C}_1 \times \text{typical energy of an α particle} \times \text{C}_2 \times \text{transfer range of α particles in UO}_2 \quad (2)$$

In which C_1 ($= 10.97 \times 10^6$ Bq cm^{-3}) is a conversion coefficient changing MBq g^{-1} (UO_2) to Bq cm^{-3} (UO_2); the typical energy of an α particle is 5.8×10^6 eV; C_2 ($= 1.6 \times 10^{-19}$ J eV^{-1}) is a conversion coefficient changing electron volts to joules, and the transfer range of α particles in UO_2 is 0.0014 cm. Given the various depths of location of α particles in UO_2, it can be calculated that only 18.8% of this energy can be absorbed by the adjacent H_2O [17].

The geometrical distribution of α-dose rate in a H_2O layer has been found to follow an exponential decay with distance from the

fuel surface [23,24]. Wu studied the influence of dose rate distributions on calculated corrosion rates, and justified the use of a simplified uniform distribution of α-dose rate [19]. Using this simplified approach, the mean dose rate to the adjacent water layer (30 μm) can be calculated to be 8.93×10^{-4} Gy s^{-1} for a 1 MBq g^{-1} (UO_2) sample according to equation (3), in which the total energy deposition is 1.425×10^{-8} J cm^{-2} s^{-1} (equation (2)), the density of water is 10^{-3} kg cm^{-3}, and the water layer thickness is 0.003 cm.

$$\text{Dose Rate}\left(\text{corresponding to}\frac{1\text{MBq}}{\text{g}\,(UO_2)}\right) = \frac{18.8\% \times \text{total energy deposition}}{\text{density of water} \times \text{water layer thickness}} \quad (3)$$

2.2. Modelling α-doped UO_2 corrosion (open system) [17]

To simulate the experiments made on α-doped UO_2 specimens we have modified our model to include only the reactions shown in Fig. 2. Here, a brief review of the reactions included in the model is presented. A more extensive discussion of these reactions has been published previously [21].

(1) The production of H_2O_2 and H_2 by water radiolysis in the radiation zone (reaction 1). This calculation considers only the radiolytic production of these two molecular species, as opposed to a full radiolysis model that would also include the radical species (e.g., OH·, H·, etc.). Our previous comparison of this calculation to the full radiolysis model showed that this simplified model overestimates the steady-state [UO_2^{2+}] (steady-state was achieved since UO_2^{2+} was allowed to escape from the system) by ~20% at the bottom of a fracture (width = 0.1 mm, depth = 1 mm); i.e., it slightly overestimates the oxidizing effect of H_2O_2 compared to the reducing effect of H_2. This makes our calculations of corrosion rates conservative.
(2) The oxidative dissolution (corrosion) of UO_2 supported by H_2O_2 reduction on the UO_2 surface (reaction 2);
(3) The decomposition of H_2O_2 to O_2 and H_2O catalyzed on the UO_2 surface (reaction 3);
(4) The reduction of dissolved UO_2^{2+} by reaction with H_2 in solution (reaction 4);
(5) The oxidative dissolution (corrosion) of UO_2 supported by O_2 reduction on the UO_2 surface (reaction 5). The cathodic reduction of O_2 is known to be slow, due to the rate controlling influence of the first electron transfer in the overall four electron reduction process [8]. For O_2 reduction on UO2 this leads to a rate 200 times slower than that for H_2O_2 reduction on UO_2, as discussed elsewhere [8].

The dissolution as UO_2^{2+} is assumed to be unimpeded by the formation on the dissolving surface of corrosion product deposits (e.g., $UO_3{\cdot}2H_2O$), which could significantly influence the corrosion rate. The avoidance of deposits would be expected in groundwater containing sufficient HCO_3^- to completely complex and dissolve the $U^{VI}O_2^{2+}$ as $U^{VI}O_2(HCO_3)_a^{(2-a)+}$.

The dissolution experiments plotted in Fig. 1 were normally performed in the oxygen-free environment anticipated inside a failed container [17]. This would constitute an open-system since the gases generated directly or indirectly by α-radiolysis, such as O_2 and H_2, would be removed. To simulate an open system in the model, the [H_2] and [O_2] at the boundary of the water layer (shown as a dashed line in Fig. 2), were set to 0. However, H_2O_2 and UO_2^{2+} would be retained within the solution, so the fluxes of these two species ($J_{H_2O_2}$, $J_{UO_2^{2+}}$) were set to 0 at this boundary. Sensitivity tests show that, while the time required to achieve a steady state depends on the thickness of the water layer, the calculated steady-state corrosion rate on the UO_2 surface does not, and a value of 1 mm was chosen as the default value in our calculations.

2.3. Modelling α-doped UO_2 corrosion (closed system)

Under the anticipated waste disposal conditions, which involve multiple barriers to inhibit transport processes, it is possible that a groundwater-containing failed container could be, at least partially, sealed by steel corrosion products, as illustrated schematically in Fig. 3. In addition, although very unlikely [25], the inner surface of the steel container could be passivated, which would eliminate the supply of redox scavengers produced by steel corrosion (Fe^{2+} and H_2), which have previously been shown to have a major influence on the redox conditions within a container [19–21]. This would

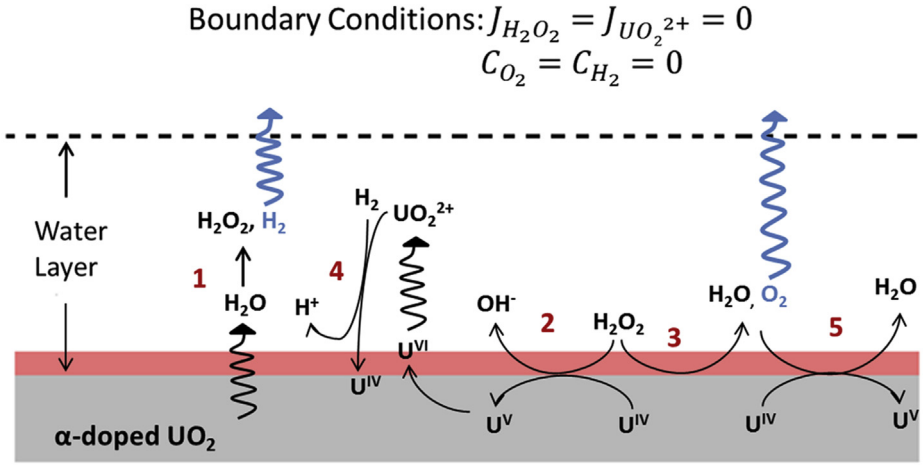

Fig. 2. Chemical reactions included in the model to simulate the corrosion of α-doped UO_2 [17]. The pink area indicates the radiation zone; i.e., the zone within which radiolytic oxidants are produced. The boundary conditions (in the figure) are applied to the boundary shown as a black dashed line. (For interpretation of the references to colour in this figure legend, the reader is referred to the web version of this article.)

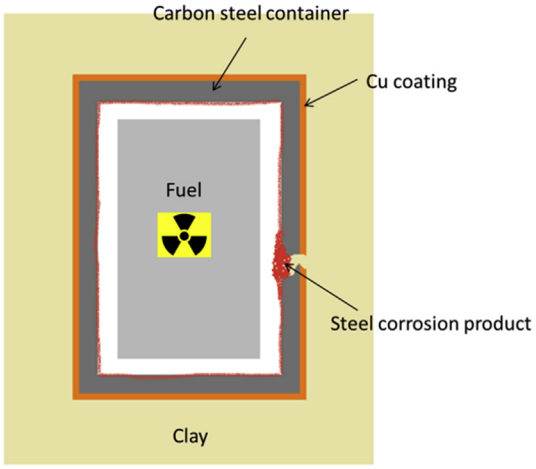

Fig. 3. Schematic showing the passivated inner surface of the steel container, and the location of the waste container failure sealed by the steel corrosion product.

constitute a closed system in which H_2 (produced by H_2O radiolysis) and O_2 (produced by the decomposition of H_2O_2) would be trapped within the container. To simulate this situation, the flux of all species ($J_{H_2O_2}$, $J_{UO_2^{2+}}$, J_{H_2}, J_{O_2}) was set to 0 on the boundary of the H_2O layer, as illustrated schematically in Fig. 4.

This model enables us to evaluate the consequences of O_2 retention in the experiments on α-doped UO_2, and also to address the consequences of the deactivation of the noble metal (ε) particles (by surface contamination or the accumulation of deposits). Many studies have shown that these particles can act as catalysts to control the rate of redox reactions on the surfaces of simulated spent fuels (SIMFUEL) [26–28].

2.4. Modelling the corrosion of spent nuclear fuel (closed system)

A less conservative and more realistic approach to evaluating the corrosion of fuel inside a resealed container is to include reactions which can occur on the surface of ε particles [29]. These particles can act as catalysts for reactions involving H_2O_2 (which would accelerate fuel corrosion) and H_2 (which would suppress corrosion) [30]. Fig. 5 shows the chemical reactions included in this model. The reactions added to those shown in Fig. 4 to address the effect of the ε particles are: (i) the oxidative dissolution (corrosion) of UO_2 supported by H_2O_2 reduction catalyzed on ε particles (reaction 2′ in Fig. 5); (ii) the reduction of oxidized surface species (U^V/U^{VI}) by H_2 oxidation on ε particles (reaction 4′ in Fig. 5); (iii) the reduction of dissolved UO_2^{2+} by reaction with H_2 on ε particles (reaction 4″ in Fig. 5); and (iv), the reaction of H_2O_2 with H_2 catalyzed by ε particles, leading to the reformation of H_2O (reaction 6 in Fig. 5).

2.5. Modelling procedure and default parameter values

The models outlined above are 1-dimensional, with the boundary conditions on the fuel surface determined by the kinetics of the surface reactions. The conditions at the water layer boundary (shown as a black dashed line in Fig. 2 and black solid lines in Figs. 4 and 5) were set to represent different scenarios. Water radiolysis can happen only in the radiation zone (domain) (shown in pink in Figs. 2, 4 and 5), while all species can diffuse in the water layer (domain) (shown in Figs. 2 and 4). The models were solved numerically using the diluted species transportation module of COMSOL Multiphysics (version 5.2a). The default values of the simulation parameters are summarized and referenced in Table 1 [20,21].

3. Results and discussion

3.1. Corrosion of α-doped UO_2 (open system)

Using the reaction scheme shown in Fig. 2, the fuel corrosion rates for different α-source strengths were calculated. As shown in Fig. 6A the calculated steady-state corrosion rates are in good agreement with the published experimental data [17], except at high α-source strengths, i.e. > 10^3 MBq g^{-1} (UO_2). At high dose rates, the corrosion rates may be governed by the formation of secondary phases, a feature which is not incorporated into the model.

In Fig. 6A, the corrosion rates are widely scattered, due to the different experimental conditions and techniques, and the large variety of fuel specimens. A more appropriate test of the model was attempted by limiting the comparison of the model calculation to corrosion rates measured on ^{233}U-doped UO_2 and ^{238}Pu-doped UO_2 specimens in deaerated solutions containing carbonate, Fig. 6B. A clearly more accurate correlation is achieved with this limited, but

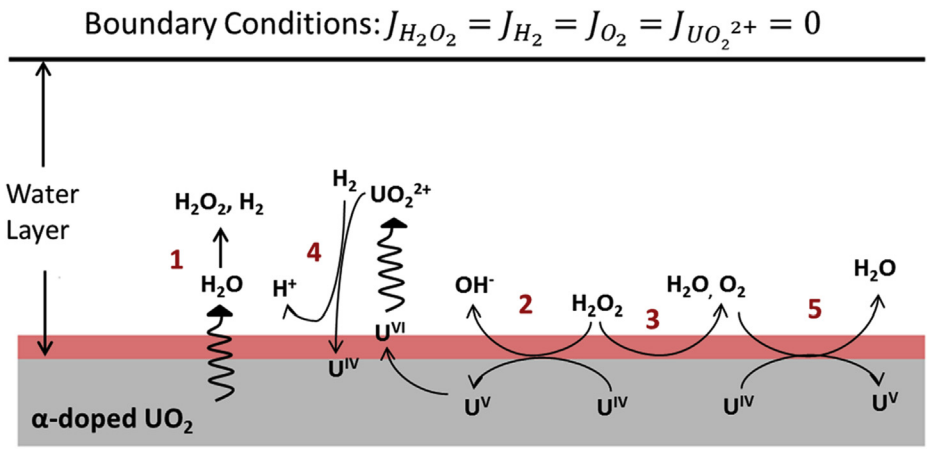

Fig. 4. Chemical reactions included in the model to simulate the corrosion of α-doped UO_2 in a closed system. The pink area indicates the radiation zone. The boundary conditions (in the figure) are applied to the boundary shown as a black line. (For interpretation of the references to colour in this figure legend, the reader is referred to the web version of this article.)

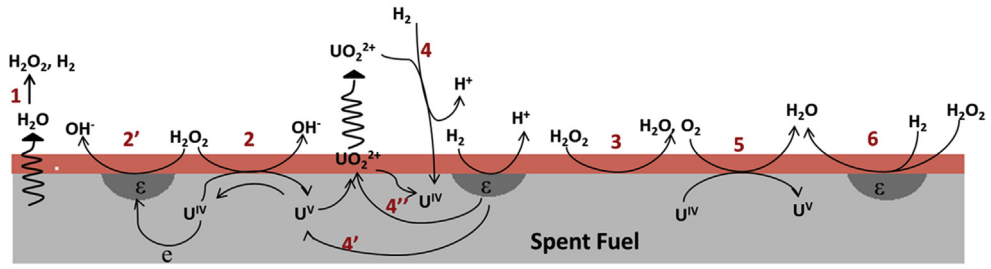

Fig. 5. Chemical reactions included in the model to simulate the corrosion of spent nuclear fuel in a closed system. The pink area indicates the radiation zone. The boundary conditions (in the figure) are applied to the boundary shown as a black line. (For interpretation of the references to colour in this figure legend, the reader is referred to the web version of this article.)

Table 1
Default values of simulation parameters.

Parameter	Symbol	Value	Units
Water layer thickness[a]	L	1	mm
Radiation zone thickness [17]	b	30	μm
ε-particle coverage	s_ε	0.01	
g-value of H_2O_2 [20]	$g_{H_2O_2}$	0.1248	μmol J^{-1}
g-value of H_2 [20]	g_{H_2}	0.1248	μmol J^{-1}
UO_2 pellet oxidation rate constant in H_2O_2 [31]	k_2	1.0×10^{-8}	m s^{-1}
H_2O_2/UO_2 surface reaction rate constant on ε [6]	k_2'	6.92×10^{-6}	m s^{-1}
H_2/UO_2^{2+} bulk reaction rate constant [32]	k_4	3.6×10^{-9}	L mol^{-1} s^{-1}
H_2/U^{VI} surface reaction rate constant on ε [33]	k_4'	4×10^{-7}	m s^{-1}
H_2/UO_2^{2+} surface reaction rate constant on ε [22],[c]	k_4''	1.3×10^{-5}	m^4 s^{-1} mol^{-1}
UO_2 pellet oxidation rate constant by O_2[b]	k_5	5×10^{-11}	m s^{-1}
H_2/H_2O_2 surface reaction rate constant on ε [22],[c]	k_6	2.8×10^{-5}	m^4 s^{-1} mol^{-1}
H_2O_2 surface-catalyzed decomposition ratio [31]		0.86	
Diffusion Coefficient of H_2O_2 [34]		2.3×10^{-9}	m^2 s^{-1}
Diffusion Coefficient of H_2 [34]		4.8×10^{-9}	m^2 s^{-1}
Diffusion Coefficient of O_2 [34]		2.4×10^{-9}	m^2 s^{-1}
Diffusion Coefficient of UO_2^{2+} [34]		7.66×10^{-10}	m^2 s^{-1}

[a] The calculated corrosion rate on the UO_2 surface is not dependent on the thickness of the water layer: 1 mm is chosen as the default value.
[b] Since studies show that the oxidation of UO_2 to $UO_{2:33}$ is ~200 times faster in H_2O_2 than in a solution containing an equal concentration of O_2 [8], k_5 is calculated based on k_2.
[c] Modified reaction rate constants [22] based on the work in Refs. [35,36].

more appropriate, data set.

In an open system, from which O_2 could be evacuated, the main oxidant driving the corrosion of UO_2 is H_2O_2, whose production rate is constant at a given α-dose rate to H_2O (equation (1)). Once the steady-state corrosion rate is established, the production and consumption of H_2O_2 will be balanced, and the $[H_2O_2]$ will be constant. Sensitivity calculations show that the rate constant for reaction 2 (k_2) does not influence the steady-state corrosion rate, only the time required to achieve it. The steady-state corrosion rate is determined by the production rate of H_2O_2 irrespective of the reactivity of the UO_2 surface.

3.2. Corrosion of α-doped UO_2 (closed system)

The good agreement between the simulated and experimental rates (Fig. 6) gives us confidence that our model can be used to simulate the consequences of various failure scenarios, in particular the closed systems described above (sections 2.3 and 2.4). Since both H_2O_2 and O_2 will cause UO_2 corrosion, the contribution to fuel corrosion will be determined by the relative concentrations of these two oxidants. For the reaction set incorporated into this model, this balance will be controlled by the rates of reaction of O_2 and H_2O_2 with UO_2 and the kinetics of the H_2O_2 decomposition reaction. Implicit in this statement is the assumption that the importance of O_2 produced by H_2O_2 decomposition will be much greater than that produced radiolytically. This assumption is justified since alpha radiolysis model calculations for deaerated water (pH = 8, alpha dose rate = 8.93×10^{-3} Gy s^{-1}) yield steady-state concentrations for H_2O_2 and O_2 of 0.003 M, and 4.2×10^{-5} M, respectively. In the model, 86% of H_2O_2 is taken to decompose, making the amount of O_2 produced by decomposition ~30 times that produced radiolytically. The corrosion rates due to H_2O_2 and O_2 can be calculated using rate equations (4) and (5), respectively.

$$R_{2,\,UO_2^{2+}} = k_2[H_2O_2] \tag{4}$$

$$R_{5,\,UO_2^{2+}} = 2k_5[O_2] \tag{5}$$

Though the mechanism of H_2O_2 decomposition is still unclear, the reaction is commonly assumed to be first-order, allowing the extent of decomposition to be expressed as a ratio.

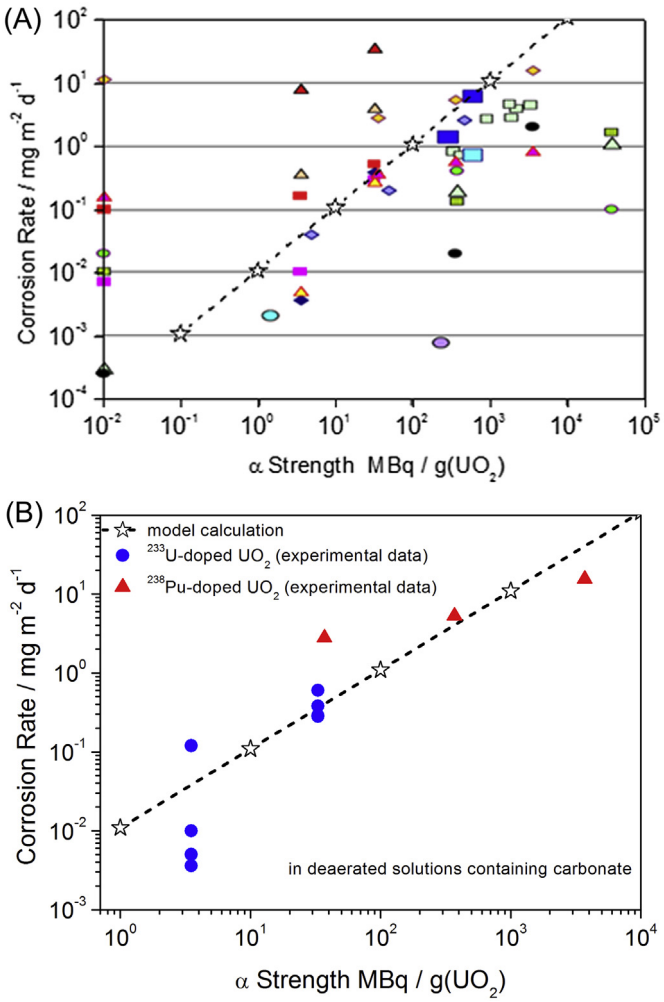

Fig. 6. Comparison of experimental corrosion rates to simulation results (stars connected by a dashed line). (A) includes the whole data set in Ref. [17]; (B) includes the data measured under similar experimental condition, i.e., for α-doped UO_2, in deaerated solutions containing carbonate.

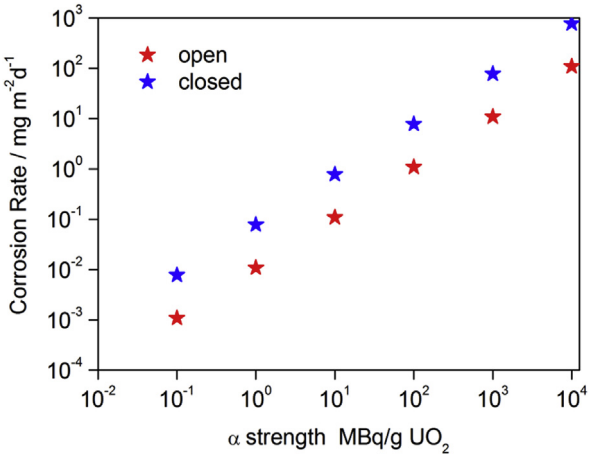

Fig. 7. Comparison of the simulated steady-state corrosion rates of α-doped UO_2 in open and closed systems.

The consequences of having a closed system were simulated using the reaction scheme shown in Fig. 4. Fig. 7 compares the simulated steady-state corrosion rates for α-doped UO_2 in open and closed systems. In a closed system, the steady-state corrosion rate is almost one order of magnitude higher, indicating that the effect of O_2 (reaction 5 in Fig. 4) should not be underestimated in a closed system. Even though the reaction rate constant for reaction 5 (UO_2 oxidation by O_2) is ~200 times smaller than that for reaction 2 (UO_2 oxidation by H_2O_2) [8], the effect of O_2 is significant, since the steady-state $[O_2]$ is higher than the $[H_2O_2]$ in a closed system. In the open system, for an α-dose rate = 8.93×10^{-3} Gy s^{-1}, the steady-state corrosion rate can be achieved in ~60 h, while ~4 years is required in the case of a closed system.

In the model, the H_2O_2 decomposition ratio is defined as the fraction or percentage of the H_2O_2 decomposed. A value of 86% for the percentage decomposed on the surface of a UO_2 pellet has been published [31]. This decomposition ratio is important in regulating the $[O_2]$ and $[H_2O_2]$ and influences the respective contributions to corrosion by the two oxidants. Table 2 summarizes the simulated $[O_2]$ and $[H_2O_2]$ (calculated by the model) when the steady-state corrosion rate is established for different H_2O_2 decomposition ratios. The corrosion rates due to H_2O_2 and O_2, calculated using equations (4) and (5), vary with the decomposition ratio as expected. However, the extent of decomposition of H_2O_2 to O_2 does not influence the total corrosion rate in a closed system. The decomposition of H_2O_2 produces O_2 ($2H_2O_2 \rightarrow 2H_2O+O_2$) as a second oxidant of UO_2 ($2UO_2 + O_2 \rightarrow 2UO_2^{2+}$). However, since the steady-state corrosion rate is dependent on the production rate of H_2O_2, the decomposition ratio will only influence the time required to reach the steady-state, which will be longer since O_2 is a more sluggish oxidant than H_2O_2.

In these calculations, the only influence of H_2 is on the reduction of UO_2^{2+} (reaction 4) [32], a reaction which will not influence radionuclide release but only lower the concentration of dissolved UO_2^{2+}. However, a significant literature is available indicating that radiolytic H_2 is reactive as a reductant on UO_2 surfaces in the presence of α-radiation. Based on the simulations by Trummer et al. [37], the α-radiolytic H_2 could decrease the steady-state concentration of H_2O_2, which will reduce the rate of α-radiation-induced dissolution of the nuclear fuel. Using a thin-layer electrochemical cell to confine the radiolysis products from an external α-source to a 25 μm layer of solution at a UO_2 disc surface (i.e., a partially closed system), Wren et al. [16] showed that, while the oxidizing influence of radiolytic H_2O_2 was dominant, the rate of surface oxidation of the UO_2 was slowed by the influence of radiolytic H_2. Traboulsi et al. [38] compared the radiolytic corrosion of UO_2 in open and closed systems in H_2O irradiated with a $^4He^{2+}$ beam and found that corrosion was significantly suppressed when H_2 was present. In both these studies only the H_2O or solution was irradiated, not the UO_2 itself. While the exact mechanism remains uncertain, the influence of H_2 was thought to involve a surface reaction. However, no usable kinetic parameters, enabling H_2 effects to be incorporated in our model, were measured.

Table 2
Comparison of the effects of H_2O_2 and O_2 on fuel corrosion for different H_2O_2 decomposition ratios, Dose rate = 8.93×10^{-3} Gy s^{-1}.

	H_2O_2 decomposition ratio		
	50%	86%	95%
$[H_2O_2]$[a]	1.67×10^{-6}	4.67×10^{-7}	1.67×10^{-7}
UO_2 corrosion rate[b] by H_2O_2	1.67×10^{-11}	4.67×10^{-12}	1.67×10^{-12}
$[O_2]$[a]	2.11×10^{-5}	3.62×10^{-5}	4.00×10^{-5}
UO_2 corrosion rate[b] by O_2	1.67×10^{-11}	2.87×10^{-11}	3.17×10^{-11}
Total UO_2 corrosion rate[c]	3.34×10^{-11}	3.34×10^{-11}	3.34×10^{-11}

[a] The unit of concentrations is mol L^{-1}, the values are calculated by the model.
[b] The unit of corrosion rates is mol m^{-2} s^{-1}, the values are calculated by equations (4) and (5).
[c] The unit of corrosion rates is mol m^{-2} s^{-1}, the value is calculated by the model.

3.3. Corrosion of spent nuclear fuel (closed system)

A number of key differences exist between α-doped UO_2 and spent fuel (commonly investigated in the form of SIMFUEL). The two key differences likely to influence fuel corrosion are lattice doping by rare earth (RE^{III}) fission products and the presence of noble metal (ε) particles. Doping with rare earths has been shown to suppress the reactivity of fuel [39,40]. However, the calculations presented in section 3.1 show that the α-radiation dose rate, which controls the rate of production of radiolytic species, is the key parameter controlling the fuel corrosion rate, making any influence of lattice doping on reactivity minor or irrelevant. By contrast, as noted above (section 2.3), the noble metal particles exert a significant influence on fuel corrosion.

The consequences of a closed system on spent fuel corrosion were simulated using the reaction scheme in Fig. 5. In this case, when reactions involving H_2 are included, a steady-state cannot be achieved. Fig. 8 shows the simulated corrosion rates calculated as a function of time using an α-dose rate of 8.93×10^{-3} Gy s^{-1} and an H_2O_2 decomposition percentage of 86%. After initially increasing rapidly, the rate begins to steadily decrease to insignificant values. Fig. 9 shows the simulated [H_2], [H_2O_2] and [O_2] at the fuel surface

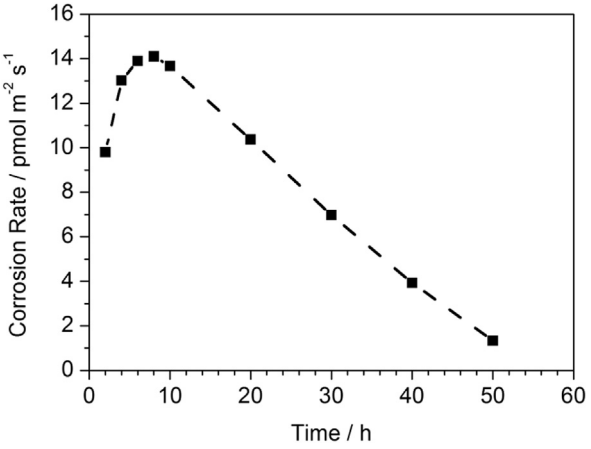

Fig. 8. Simulated corrosion rates of spent nuclear fuel (α-dose rate = 8.93×10^{-3} Gy s^{-1}) as a function of time. All other model parameters have the default values (Table 1).

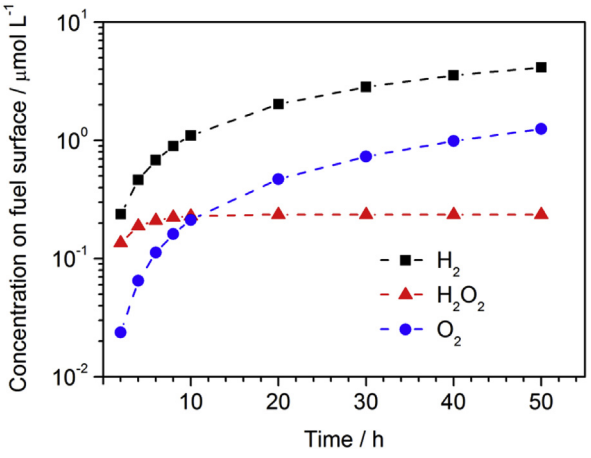

Fig. 9. Simulated [H_2], [H_2O_2] and [O_2] at the fuel surface (α-dose rate = 8.93×10^{-3} Gy s^{-1}) as a function of time. All other model parameters have the default values (Table 1).

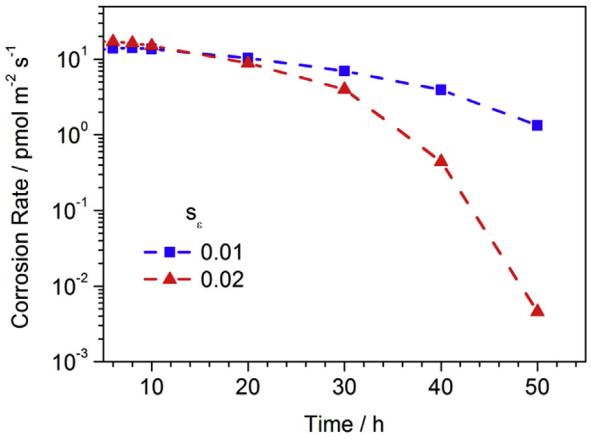

Fig. 10. Simulated corrosion rates of spent nuclear fuel (α-dose rate = 8.93×10^{-3} Gy s^{-1}) as a function of time for different ε-particle coverages. All other model parameters have the default values (Table 1).

for the same dose rate. Over the first 10 h, the accumulation of H_2 is insufficient to overcome the oxidizing effect of H_2O_2, resulting in the increase in corrosion rate. With time, as the [H_2] increases, the corrosion rate is suppressed. After 50 h, the [H_2] at the fuel surface is ~20 times the [H_2O_2]. In addition, despite the [O_2] at the fuel surface being ~5 times that of [H_2O_2] after 50 h, H_2O_2 remains the dominant oxidant due to the high rate constant for its reaction with UO_2 compared to that of O_2.

These results clearly demonstrate that the accumulation of radiolytic H_2 in a closed system will radically suppress the fuel corrosion by reducing the oxidized UO_2 surface (reactions 4′ and 4″ shown in Fig. 5) and consuming H_2O_2 (reaction 6 shown in Fig. 5). This is consistent with the experimental results of Carbol et al. [41] who conducted a long term corrosion experiment on spent fuel under an overpressure of 3.2 bar of H_2 and found that the measured uranium concentration coincided with the calculated UO_2 solubility, indicating that the dissolution is solubility-controlled; i.e., not radiolytically driven. Also, Trummer et al. [6] showed, in a N_2 purged solution, that the presence of 3 wt % Pd (as a surrogate for ε-particles) could prevent corrosion when only radiolytically produced H_2 was present.

Fig. 10 compares the simulated corrosion rates as a function of time for different coverages by ε-particles, which can catalyze both H_2O_2 reduction and H_2 oxidation reactions. The availability of ε-particles will be determined by the extent of fuel burnup. At short times there is a slight increase in corrosion rate, since H_2O_2 initially plays a dominant role in controlling the surface redox conditions, with Reaction 2′ (Fig. 5) being accelerated, leading to the increased corrosion rate. However, at longer times, as the [H_2] increases, the increased surface area of available ε particles allows reactions 4′ and 4″ (Fig. 5) to dominate, leading to a very rapid decrease in corrosion rate.

4. Conclusions

In this study, the calculated steady-state corrosion rates are in good agreement with published dissolution rates measured on a range of α-doped UO_2 and spent fuel specimens.

The value of the rate constant for the reaction of H_2O_2 with UO_2 does not influence the calculated steady-state corrosion rate, only the time required to achieve the steady-state value. This demonstrates that the corrosion rate is determined by the radiolytic production rate of H_2O_2, irrespective of the reactivity of the fuel surface.

Calculations of corrosion rates for α-doped UO_2 in a closed system demonstrate that the accumulation of O_2, primarily from H_2O_2 decomposition, would lead to an increase in corrosion rate. This reflects the fact that, even though the rate constant for the reaction of O_2 is ~200 times less than that of H_2O_2, the effect of O_2 can be significant since the steady-state $[O_2]$ can be greater than that of H_2O_2 in a closed system. However, this calculation does not include the influence of radiolytic H_2, which will suppress the corrosion rate.

When the influence of H_2 as a reductant reacting on noble metal (ε) particles is included, the model can be used to predict the corrosion rates of spent fuel. No steady-state can be established due to the accumulation of radiolytic H_2 with time, the corrosion rate decreasing with time to a negligible level (i.e., $<10^{-20}$ mol m^{-2} s^{-1}). The dose rate, H_2O_2 decomposition ratio, and the coverage of ε particles will influence the time needed for the corrosion rate to decrease to a negligible level, but will not prevent the suppression of the fuel corrosion rate.

Acknowledgment

This research was funded under the Industrial Research Chair agreement between the Natural Sciences and Engineering Research Council (NSERC, Ottawa) and the Nuclear Waste Management Organization (NWMO, Toronto). We are grateful to the authors of reference [17] for permission to include Figs. 1 and 6. We thank Dr. Jiju Joseph and Ryan P. Morco for conducting simulations using FACSIMILE.

References

[1] Choosing a Way Forward: the Future Management of Canada's Used Nuclear Fuel, Nuclear Waste Management Organization, Toronto, 2005. http://www.nwmo.ca.
[2] Implementing Adaptive Phased Management 2016 to 2020, Nuclear Waste Management Organization, Toronto, 2016. http://www.nwmo.ca.
[3] J. McMurry, D.A. Dixon, J.D. Garroni, B.M. Ikeda, S. Stroes-Gascoyne, P. Baumgartner, T.W. Melnyk, Evolution of a Canadian Deep Geologic Repository: Base Scenario, 06819-REP-01200-10092-R00, Ontario Power Generation, Toronto, 2003.
[4] D.W. Shoesmith, F. King, B.M. Ikeda, An Assessment of the Feasibility of Indefinite Containment of Canadian Nuclear Fuel Wastes, AECL-10972 COG-94–534, 1995.
[5] F. King, M. Kolar, The Copper Container Corrosion Model Used in AECL's Second Case Study, 06819-REP-01200-10041-R00, Ontario Power Generation, Toronto, 2000.
[6] M. Trummer, O. Roth, M. Jonsson, H_2 inhibition of radiation induced dissolution of spent nuclear fuel, J. Nucl. Mater. 383 (3) (2009) 226–230.
[7] E. Ekeroth, O. Roth, M. Jonsson, The relative impact of radiolysis products in radiation induced oxidative dissolution of UO_2, J. Nucl. Mater. 355 (1–3) (2006) 38–46.
[8] D.W. Shoesmith, Fuel corrosion processes under waste disposal conditions, J. Nucl. Mater. 282 (2000) 1–31.
[9] K. Ollila, E. Myllykylä, M. Tanhua-Tyrkkö, T. Lavonen, Dissolution rate of alpha-doped UO_2 in natural groundwater, J. Nucl. Mater. 442 (1–3) (2013) 320–325.
[10] S. Stroes-Gascoyne, F. Garisto, J.S. Betteridge, The effects of alpha-radiolysis on UO_2 dissolution determined from batch experiments with ^{238}Pu-doped UO_2, J. Nucl. Mater. 346 (1) (2005) 5–15.
[11] T. Mennecart, C. Cachoir, K. Lemmens, Influence of the alpha radiation on the UO_2 dissolution in high pH cementitious waters, J. Radioanal. Nucl. Chem. 304 (1) (2014) 61–66.
[12] K. Ollila, Influence of Radiolysis on UO_2 Fuel Matrix Dissolution under Disposal Conditions, Working Report 2011-27, POSIVA OY, EURAJOKI, 2011.
[13] T. Mennecart, B. Grambow, M. Fattahi, Z. Andriambololona, Effect of alpha radiolysis on doped UO_2 dissolution under reducing conditions, Radiochim. Acta 92 (2004) 611–615.
[14] V.V. Rondinella, Hj. Matzke, J. Cobos, T. Wiss, Leaching behaviour of UO_2 containing α-emitting actinides, Radiochim. Acta 88 (2000) 527–531.
[15] J. Cobos, L. Havela, V.V. Rondinella, J. Pablo, T. Gouder, J.P. Glatz, P. Carbol, H. Matzke, Corrosion and dissolution studies of UO_2 containing α-emitters, Radiochim. Acta 90 (2002) 597–602.
[16] J.C. Wren, D.W. Shoesmith, S. Sunder, Corrosion behavior of uranium dioxide in alpha radiolytically decomposed water, J. Electrochem. Soc. 152 (11) (2005) B470–B481.
[17] C. Poinssot, C. Ferry, M. Kelm, B. Grambow, A. Marttinez, L. Johnson, Z. Andriambololona, J. Bruno, C. Cachoir, J.M. Cavedon, H. Christensen, C. Corbel, C. Jegou, K. Lemmens, A. Loida, P. Lovera, F. Miserque, J. De Pablo, A. Poulesquen, J. Quinones, V. Rondinella, K. Spahiu, D.H. Wegen, Spent Fuel Stability under Repository Conditions – Final Report of the European Project, European Commission Report CEA-R-6093, 2005.
[18] M. Gobien, F. Garisto, E. Kremer, Fifth Case Study: Reference Data and Codes, NWMO TR-2013-05, Nuclear Waste Management Organization, Toronto, 2013.
[19] L. Wu, Y. Beauregard, Z. Qin, S. Rohani, D.W. Shoesmith, A model for the influence of steel corrosion products on nuclear fuel corrosion under permanent disposal conditions, Corros. Sci. 61 (2012) 83–91.
[20] L. Wu, N. Liu, Z. Qin, D.W. Shoesmith, Modeling the radiolytic corrosion of fractured nuclear fuel under permanent disposal conditions, J. Electrochem. Soc. 161 (8) (2014) E3259–E3266.
[21] L. Wu, Z. Qin, D.W. Shoesmith, An improved model for the corrosion of used nuclear fuel inside a failed waste container under permanent disposal conditions, Corros. Sci. 84 (2014) 85–95.
[22] N. Liu, L. Wu, Z. Qin, D.W. Shoesmith, Roles of radiolytic and externally generated H_2 in the corrosion of fractured spent nuclear fuel, Environ. Sci. Technol. 50 (22) (2016) 12348–12355.
[23] M. Jonsson, F. Nielsen, O. Roth, E. Ekeroth, S. Nilsson, M.M. Hossain, Radiation induced spent nuclear fuel dissolution under deep repository conditions, Environ. Sci. Technol. 41 (2007) 7087–7093.
[24] F. Nielsen, M. Jonsson, Geometrical α- and β-dose distributions and production rates of radiolysis products in water in contact with spent nuclear fuel, J. Nucl. Mater. 359 (1–2) (2006) 1–7.
[25] S.L.W. Hill, N. Liu, Z. Qin, D. Zagidulin, D.W. Shoesmith, Interactions between carbon steel and UO_2 corrosion fronts inside a failed nuclear waste container, in: 17th International Conference on Environmental Degradation of Materials in Nuclear Power Systems – Water Reactors, 2015. Ottawa, Ontario, Canada.
[26] M.E. Broczkowski, P.G. Keech, J.J. Noël, D.W. Shoesmith, Corrosion of uranium dioxide containing simulated fission products in dilute hydrogen peroxide and dissolved hydrogen, J. Electrochem. Soc. 157 (8) (2010) C275–C281.
[27] H. He, M. Broczkowski, K. O'Neil, D. Ofori, O. Semenikhin, D.W. Shoesmith, Corrosion of Nuclear Fuel (UO_2) inside a Failed Nuclear Waste Container, NWMO TR-2012-09, Nuclear Waste Management Organization, Toronto, 2012.
[28] M. Razdan, D.W. Shoesmith, The influence of hydrogen peroxide and hydrogen on the corrosion of simulated spent nuclear fuel, Faraday Discuss. 180 (2015) 283–299.
[29] D.W. Shoesmith, Used Fuel and Uranium Dioxide Dissolution Studies – a Review, NWMO TR-2007-03, Nuclear Waste Management Organization, Toronto, 2007.
[30] M.E. Broczkowski, J.J. Noël, D.W. Shoesmith, The inhibiting effects of hydrogen on the corrosion of uranium dioxide under nuclear waste disposal conditions, J. Nucl. Mater. 346 (1) (2005) 16–23.
[31] R. Pehrman, M. Trummer, C.M. Lousada, M. Jonsson, On the redox reactivity of doped UO_2 pellets – influence of dopants on the H_2O_2 decomposition mechanism, J. Nucl. Mater. 430 (1–3) (2012) 6–11.
[32] E. Ekeroth, M. Jonsson, T.E. Eriksen, K. Ljungqvist, S. Kovács, I. Puigdomenech, Reduction of UO_2^{2+} by H_2, J. Nucl. Mater. 334 (1) (2004) 35–39.
[33] M. Trummer, S. Nilsson, M. Jonsson, On the effects of fission product noble metal inclusions on the kinetics of radiation induced dissolution of spent nuclear fuel, J. Nucl. Mater. 378 (1) (2008) 55–59.
[34] A. Elliot, Rate Constants and G-values for the Simulation of the Radiolysis of Light Water over the Range 0-300°C, AECL-11073 COG-94-167, 1994.
[35] S. Nilsson, M. Jonsson, On the catalytic effect of Pd(s) on the reduction of UO_2^{2+} with H_2 in aqueous solution, J. Nucl. Mater. 374 (1–2) (2008) 290–292.
[36] S. Nilsson, M. Jonsson, On the catalytic effects of UO_2(s) and Pd(s) on the reaction between H_2O_2 and H_2 in aqueous solution, J. Nucl. Mater. 372 (2–3) (2008) 160–163.
[37] M. Trummer, M. Jonsson, Resolving the H_2 effect on radiation induced dissolution of UO_2-based spent nuclear fuel, J. Nucl. Mater. 396 (2010) 163–169.
[38] A. Traboulsi, J. Vandenborre, G. Blain, B. Humbert, J. Barbet, M. Fattahi, Radiolytic corrosion of uranium dioxide: role of molecular species, J. Phys. Chem. C. 118 (2) (2014) 1071–1080.
[39] M. Razdan, D.W. Shoesmith, The electrochemical reactivity of 6.0 wt% Gd-doped UO_2 in aqueous carbonate/bicarbonate solutions, J. Electrochem. Soc. 161 (4) (2014) H225–H234.
[40] D.W. Shoesmith, The chemistry/electrochemistry of spent nuclear fuel as a wasteform, in: P.C. Burns, G.E. Sigmon (Eds.), Uranium: Cradle to Grave, Mineralogical Society of Canada, Québec, 2013.
[41] P. Carbol, J. Cobos-Sabate, J.-P. Glatz, C. Ronchi, V. Rondinella, D.H. Wegen, T. Wiss, A. Loida, V. Metz, B. Kienzler, K. Spahiu, B. Grambow, J. Quinones, A. Martinez Esparza Valiente, The Effect of Dissolved Hydrogen on the Dissolution of ^{233}U Doped UO_2(s), High Burn-up Spent Fuel and MOX Fuel, SKB TR-05–09, Swedish Nuclear Fuel and Waste Management Co, Stockholm, 2005.